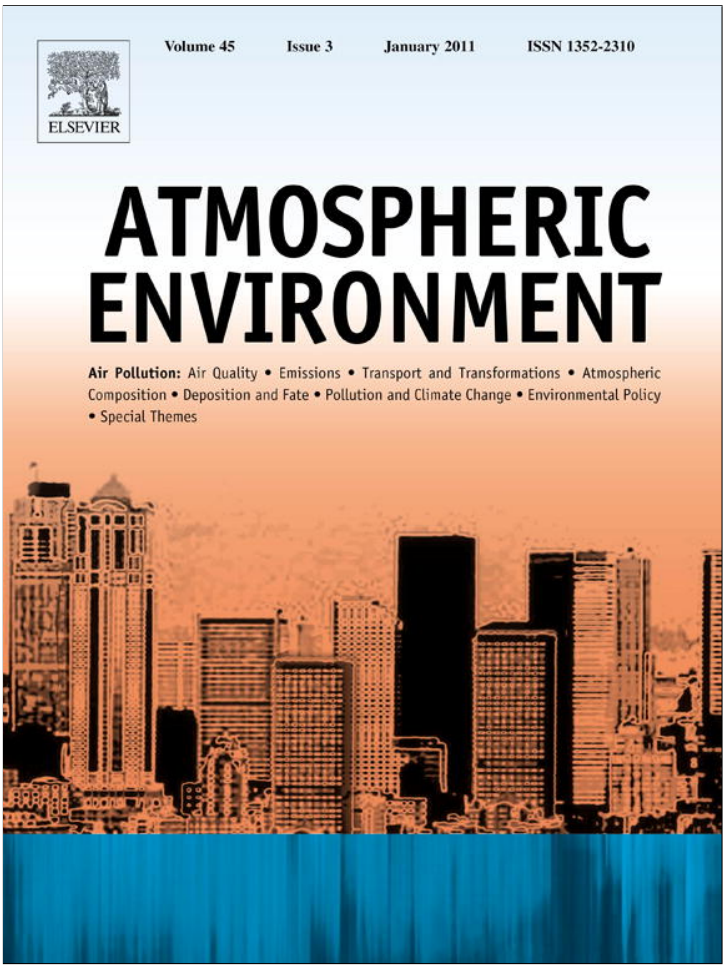

Atmospheric Environment 45 (2011) 716–726

Contents lists available at ScienceDirect

Atmospheric Environment

journal homepage: www.elsevier.com/locate/atmosenv

Satellite monitoring of the biomass-burning aerosols during the wildfires of August 2007 in Greece: Climate implications

D.G. Kaskaoutis [a,*], Shailesh Kumar Kharol [b], N. Sifakis [c], P.T. Nastos [d], Anu Rani Sharma [b], K.V.S. Badarinath [b], H.D. Kambezidis [a]

[a] Atmospheric Research Team, Institute for Environmental Research and Sustainable Development, National Observatory of Athens, Lofos Nymphon, P.O. Box 20048, GR-11810 Athens, Greece
[b] Atmospheric Science Section, Oceanography Division, National Remote Sensing Centre (Dept. of Space-Govt. of India), Balanagar, Hyderabad 500 625, India
[c] Institute for Space Application and Remote Sensing, National Observatory of Athens, Palaia Penteli, GR-15236 Athens, Greece
[d] University of Athens, Department of Geology and Geoenvironment, University campus, GR-15784 Athens, Greece

ARTICLE INFO

Article history:
Received 13 April 2010
Received in revised form
17 September 2010
Accepted 21 September 2010

Keywords:
Forest fires
Remote sensing
Biomass burning
Radiative forcing
Peloponnese
Greece

ABSTRACT

Biomass burning and associated emissions of aerosols into the atmosphere play a vital role in atmospheric composition and climate change. During summer of 2007, Greece faced the worst natural disaster recorded in recent decades in terms of human losses, number of fire outbreaks and extent of the estimated burned area (more than 12% of the total forested areas in Greece). The present study aims at analyzing the impact of these fire events in western Peloponnese on atmospheric aerosol concentrations using satellite data. MODIS-derived Aerosol Optical Depth (AOD), effective radius, Ångström exponent, mass concentration, cloud-condensation nuclei (CCN) and OMI Aerosol Index (AI), single scattering albedo, absorption and extinction optical depths were analyzed. MODIS data showed smoke plumes traversing thousands of kilometers southwards influencing the central Mediterranean as well as the north African coastal regions. These thick smoke plumes dramatically affected AOD and aerosol-mass concentrations over the region and altered the microphysical aerosol properties, such as the effective radius and absorption coefficient. Model calculations suggested that the shortwave radiation at the ground was reduced by ~50 Wm^2, while that at the top of the atmosphere was reduced by ~20 Wm^2 resulting in atmospheric heating of ~30 Wm^2 over the areas affected by the smoke plumes.

1. Introduction

Forests are one of the most important natural resources and aspects of the earth's biosphere owing to their multifunction characteristics. Forest fires have become a basic threat to the environment in many parts of the world. Tropical forest fires and biomass burning are significant sources of carbon in the atmosphere producing large amounts of trace gases and aerosols, which play a pivotal role in tropospheric chemistry and global climate (e.g. Reid et al., 1999). Fossil fuel and biomass burning are major sources of aerosols, which are often transported to hundreds of kilometers downwind (Balis et al., 2003) affecting air quality, atmospheric chemistry, radiation balance and acid deposition (e.g. Turquety et al., 2009). Biomass-burning aerosols strongly absorb or reflect the incoming radiation, thereby reducing the amount of sunlight reaching the earth's surface. Furthermore, the radiative effect of smoke must be taken into account to predict adequately the overall impact of aerosols on local weather and regional climate because the heating caused by smoke alters atmospheric dynamics and thermodynamics (Satheesh and Krishnamoorthy, 2005). Biomass burning is now recognized to be a major contribution to the global emissions of trace gases and aerosols (Badarinath et al., 2004, 2009a,b), but also in the northern mid-latitudes (Andreae and Merlet, 2001; Westerling et al., 2003; Kasischke et al., 2005).

Satellite-remote sensing is a well-established tool for monitoring wildfires, mapping the burned areas and evaluating biomass-burning aerosols via modeling (e.g., Amiridis et al., 2009; Minchella et al., 2009). Kontoes et al. (2009) have mapped the burned areas in Greece for the year 2007 using a variety of satellite data in the framework of ESA's RISK EOS European programme. The NASA Moderate Resolution Imaging Spectroradiometer (MODIS) is used systematically to generate a suite of products including a 1-km active fire product (http://rapidfire.sci.gsfc.nasa.gov/), and more recently a burned area product at 500-m resolution (Giglio et al., 2003; Roy et al., 2005). MODIS can also be used to estimate the optical depth of aerosols from wildfires (e.g. Tanré et al., 1997).

* Corresponding author.
E-mail address: dkask@meteo.noa.gr (D.G. Kaskaoutis).

1352-2310/$ – see front matter © 2010 Elsevier Ltd. All rights reserved.
doi:10.1016/j.atmosenv.2010.09.043

Satellite observations of atmospheric trace gases and aerosols in fire plumes are also necessary to evaluate model simulations of their effects. On the other hand, the signatures of biomass burning constitute the main feature of the global CO distributions observed from space (e.g. McMillan et al., 2008; Turquety et al., 2008).

In summer, the Mediterranean Basin is often affected by large wildfires, but the associated emissions are not always included in air quality models. The prime objective of the present study is to understand the impact of forest fires on atmospheric aerosol concentrations, optical properties and their climate impact over the southwestern region of Greece (Peloponnese) and adjoining seas. Greece is located in the Mediterranean with favorable conditions for forest fires in summer (Kambezidis et al., 2006). The fires occurred in Greece in the summer of 2007 created high concentrations of biomass-burning aerosols as well as large spatial extent of the biomass smoke and significant climate implications over the area comparable in magnitude with those observed during forest fires in India (e.g. Badarinath et al., 2009a,b).

2. Study area

Peloponnese is a peninsula situated in the southern part of the Greek mainland with lots of agricultural activities (Fig. 1) covering an area of 21,549 km^2. The climatic data over the region show that risk for forest fires increased dramatically during summer 2007 with hot and permanent heat waves and positive temperature anomalies following a dry winter (Founda and Giannakopoulos, 2009) causing extensive fires in Greece as well as in Albania and southern Italy as shown by the MODIS fire locations (Fig. 1a) in the period 15–31 August 2007. Fig. 1b, taken from the Aqua-MODIS sensor on 25 August 2007 shows the intense smoke plumes from the extended burned areas in western Peloponnese, which reveal

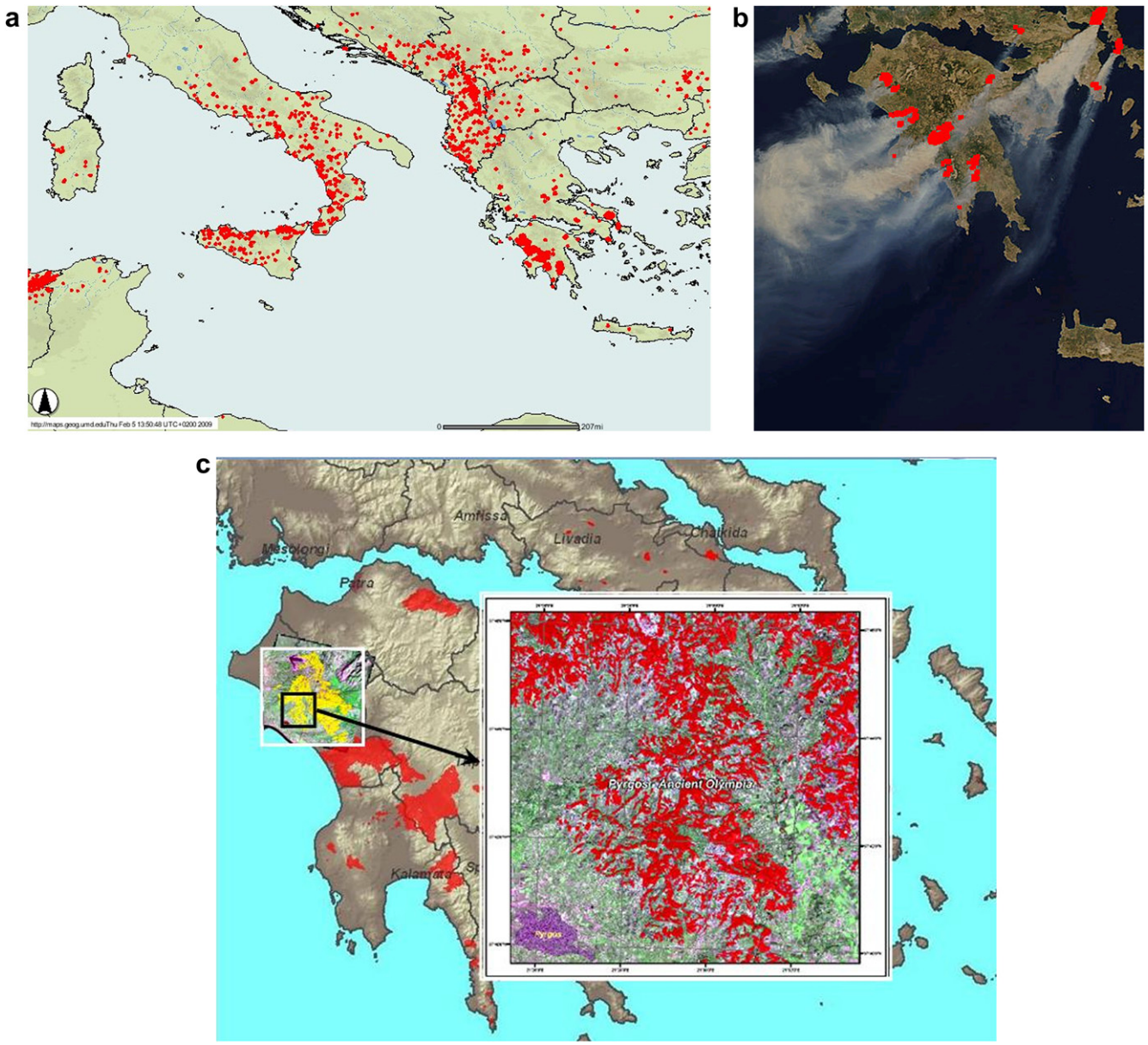

Fig. 1. Satellite mapping of the fire events over coastal Mediterranean and Greece in August 2007. (a) Fire events in the period 15–31 August 2007 as derived from MODIS fire counts website (http://maps.geog.umd.edu/firms/). (b) Satellite image from the Aqua-MODIS sensor above southern Greece on 25 August 2007. (c) The burned areas in Peloponnese focusing more on the area of Ancient Olympia during late August 2007 as mapped by the very high-resolution FORMOSAT-2 data.

the great natural hazard over the area being the subject of many studies (Boschetti et al., 2008; Wang et al., 2008; Liu et al., 2009; Turquety et al., 2009; Veraverbeke et al., 2010a,b). The plumes from those fires covered a large area above south Ionian Sea and central Mediterranean and were transported thousands of kilometers downwind.

More than 60 people lost their lives, large areas covered with natural vegetation, farmlands and olive groves were destroyed and much of the area's infrastructure was burned down. Also, significant monuments of world cultural heritage, such as Olympia, the home of the ancient Olympics, suffered severe damage. The total area burnt in Peloponnese in August 2007 was estimated to 116,496 ha (Kontoes et al., 2008). The very high-resolution FORMOSAT-2 satellite data with a 2-m spatial resolution (Kontoes et al., 2009) were used for Burn Scar Mapping in Peloponnese and particularly the sensitive archaeological site of Olympia (Fig. 1c). Using this very high-resolution image the burned areas in the most forest-fire-affected prefecture of Ilia were estimated to 45,341 ha. Boschetti et al. (2008) found that the MODIS-burned-area product (MCD45) estimated 292,657 ha from 22 June to 30 August 2007 across Greece, while EFFIS (European Forest Fires Information Service) reported 272,163 ha. Approximately 12% of the Natura 2000 protected sites in Peloponnese were affected by the wildfires (WWF Hellas, 2008).

Although the number of fires was similar to that of previous years, the severity of the fire events was greater in August 2007 due to several heat waves in the preceding period, extended droughts and strong winds. The patterns of the daily mean and anomalies (mean minus the total mean of the period 1968–1996) of the wind vectors (ms^{-1}) on 25 August 2007, from NCEP/NCAR Reanalysis are depicted in Fig. 2, left and right panels respectively. The wind pattern was a northeastern current (called Etesians) towards Greece with gusts reaching 13 ms^{-1} (left panel) in the region of Peloponnese. These meteorological conditions with respect to wind speed exceeded the climatological normal (period 1968–1996) by ~13 ms^{-1} (right panel) in the wider region of Peloponnese, indicating that the prevailing wind current was strong enough. Similar wind vector patterns were apparent from the lower to the middle troposphere, indicating a northeastern current towards Greece (not shown). This weather type is established when a north Atlantic anticyclone extended over Europe covering the Balkans is combined with the Indian low extended over Asia Minor and eastern Mediterranean Sea. The blow of Etesians winds transfers polar continental (cP) air masses to northern Greece and the result is the summer drought and the uniform weather conditions (Nastos et al., 2002). Those prevailing northeasterly winds transported the smoke plumes from the wildfires in Peloponnese over large distances (reaching north African coast).

3. Data set

The OMI on board the Aura satellite was launched in July 2004 and flies as part of the NASA A-train constellation (Levelt et al., 2006). It has a ground-spatial resolution of 13 × 24 km at nadir and uses a retrieval algorithm similar to the one used by TOMS (Torres et al., 1998). The OMAERUV aerosol algorithm used in this work utilizes the backscattered radiances measured at 354 and 388 nm to retrieve UV Aerosol Index, Aerosol Optical Depth (AOD) and absorption aerosol optical depth (AAOD) at 354 nm. The OMAERUV algorithm uses pre-computed top of the atmosphere (TOA) reflectances for a set of 21 assumed aerosol models to retrieve AOD and AAOD. The set of aerosol models is composed of three major aerosol types: desert dust, carbonaceous aerosols from biomass burning, and weakly absorbing aerosols. Each type includes seven models with different single-scattering albedos (SSA). Great efforts have been made focusing on validating the OMI algorithms, and comparing the OMI products with ground-based retrievals (e.g. Curier et al., 2008; Arola et al., 2009). In the present study we use the Aura-OMI daily aerosol products (AI, extinction and absorption optical depths, SSA, NO_2 troposheric amount), which are Level-3 global gridded products generated by binning the original pixels from the Level-2 data (15 orbits per day, 13 × 24 km spatial resolution) into a 0.25° × 0.25° grid.

MODIS provides several aerosol parameters over land and ocean by means of two different algorithms. The uncertainties in determining aerosol parameters are different for each algorithm (Remer et al., 2005) and are mainly attributed to non-spherical particles and the sub-pixel cloud contamination. In this study Collection-5 (C005) Level-3 products (Levy et al., 2007) with a 1° × 1° spatial resolution were used from http://giovanni.gsfc.nasa.gov/. The MODIS products used are AOD, Ångström exponent in the 550–865-nm band, effective radius, mass concentration, Cloud-Condensation Nuclei (CCN) and water vapor content.

MOPITT employs gas correlation spectroscopy to measure thermal and reflected infrared radiances. It measures energy in three absorption bands: 2.3 μm and 2.4 μm to extract column CH_4 and CO, respectively, and 4.7 μm to derive CO profiles. Global gridded maps of CO and CH_4 distribution have been generated to

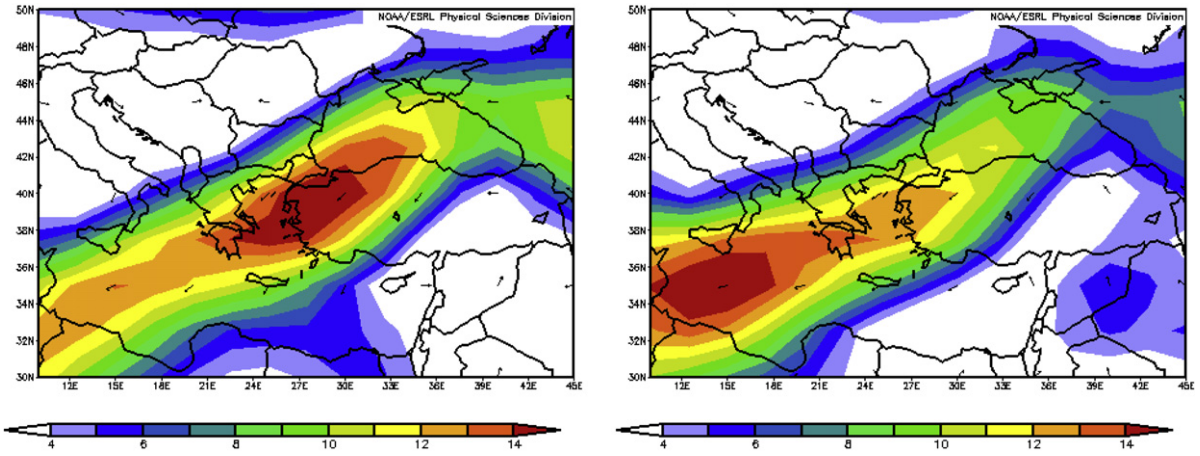

Fig. 2. Spatial distribution of the daily mean wind vectors (ms^{-1}) (left panel) and of the daily anomalies (mean − total mean of the period 1968–1996) at 850 hPa, on 25 August 2007, from NCEP/NCAR re-analysis.

help test and refine models that describe mainly biomass burning and agricultural sources, and provide indirect information on chemical processes. A new version of the MOPITT retrieval algorithm is currently being developed in order to reduce the apparent high bias (between 5% and 7% on the total column) of the background retrievals by comparison with in-situ observations (Emmons et al., 2007).

4. Results and discussion

4.1. Temporal variation of biomass-burning aerosol properties

Fig. 3 shows the daily OMI observations during August 2007. This area includes the western part of Peloponnese and the southern Ionian Sea. The most characteristic OMI products for the detection of a fire event are presented here, e.g. extinction and absorption optical depths at 354 nm, SSA, NO_2 tropospheric column density and AI. The mean extinction optical depth (Fig. 3a) varies from low (0.16) to high (1.17), with a mean value of 0.42 ± 0.24 during August 2007. High values were observed during the fire period (24–27 August) because of the dominance of accumulation-mode particles, which cause larger increase in AOD at shorter wavelengths (Kaskaoutis et al., 2007; Radhi et al., 2009). Note also the larger standard deviations on the fire-event days caused by the large heterogeneity in the spatial distribution of the smoke plume. Therefore, over the gridded points affected by intense smoke plume the extinction optical depth can be much higher than 3.0, a value that is larger than those presented during biomass burning in Amazonia (Reid et al., 1999), South Africa (Eck et al., 2001, 2003) and Australia (Radhi et al., 2009). Regarding the absorption optical depth (Fig. 3b), its area-averaged values present a similar temporal variation to that of extinction. Thus, very high (0.10–0.16) mean values are presented in the burning period, which reach 1.0, indicating the strong absorbing nature of the biomass-burning

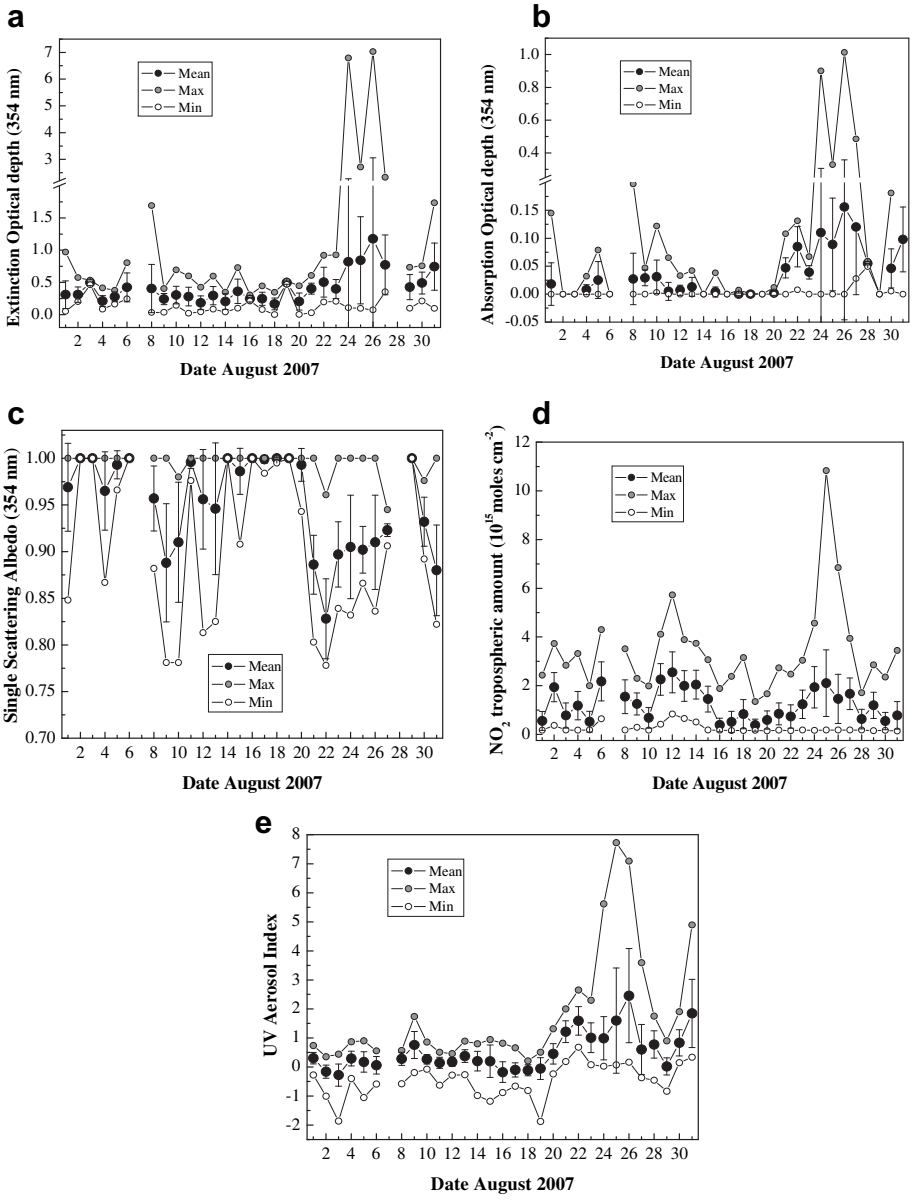

Fig. 3. Day-to-day variation of (a) extinction optical depth, (b) absorption optical depth, (c) Single Scattering Albedo, (d) NO_2 tropospheric column and (e) AI derived by OMI during August 2007. The mean, standard deviation, maximum and minimum values correspond to the area 34.5°–38.5°N and 18°–22°E.

aerosols. On the other hand, in the pre-burning period the absorption optical depth at 354 nm is very low (<0.02).

In the OMAERUV algorithm the accuracy of SSA is mainly determined by the aerosol models to represent the real aerosols; the SSA accuracy was estimated at 0.05–0.10 (ATBD-OMI, 2002). Nevertheless, the temporal variation shows that SSA exhibits lower values, as expected, during the burning period (Fig. 3c). NO_2, an anthropogenic-activity and biomass-burning gas, exhibited large day-to-day variations (Fig. 3d). Large NO_2 amounts were observed in the beginning of the period (e.g. 6 and 11–15 August) mainly attributed to anthropogenic emissions. Note that on these dates both AOD and AI did not present large values indicating a low-to-moderate aerosol load, while SSA is lower and indicative of anthropogenic influence. The NO_2 amount started to increase in the burning period, with maximum values detected above the smoke-plume stream.

AI exhibited low mean values until 20 August, and a large increase during the burning period, reaching 2.5 on 26 August, indicative of the presence of UV-absorbing aerosols, such as soot and carbonaceous particles (Fig. 3e). This value is higher than that during the biomass-burning period in the south-African savanna regions (Eck et al., 2003). During the burning period the AI maximum values were larger than 6.0 in the intense smoke plume. Over few days the mean AI was negative indicating the dominance of non-absorbing aerosols over the area.

Fig. 4 shows the temporal variability of several aerosol properties obtained from Aqua-MODIS during August 2007. Moderate-to-high AOD_{550} values occurred in August 2007 (0.25 ± 0.08) (Fig. 4a), since the lifetime of atmospheric aerosols is sufficiently long in this season with absence of precipitation. The regionally-averaged AOD_{550} shows a consistent increase during the last days of August 2007 (from 0.35 to 0.5) due to the extent of fire events. The mean AOD_{550} as well as its spatial distribution exhibited larger variation during the forest-fire period. Badarinath et al. (2004) found large variations in AOD, ranging from 0.1 to 4.2, while precipitable water vapor ranged from 0.7 to 1.8 g cm^{-3} in northeastern India during

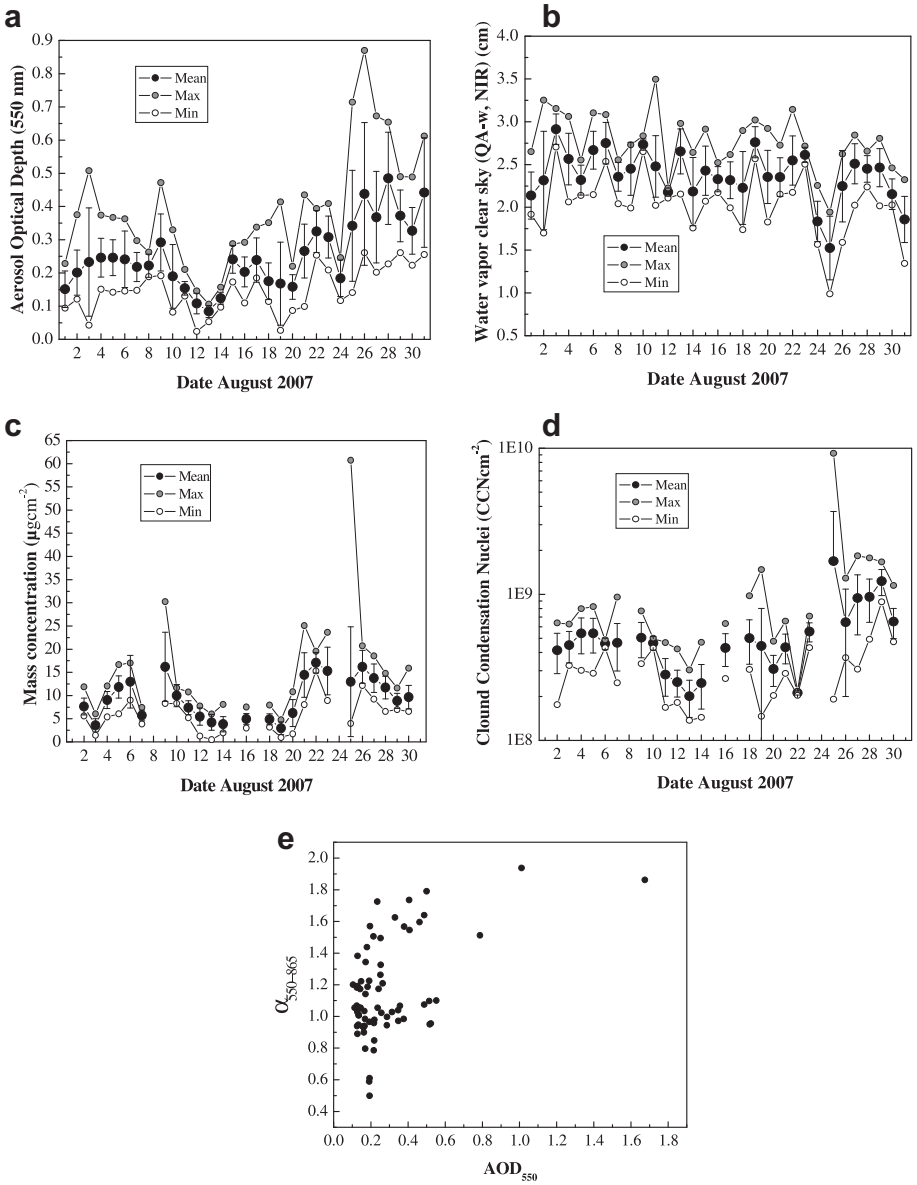

Fig. 4. Day-to-day variation of (a) AOD_{550}, (b) water vapor content, (c) aerosol-mass concentration, and (d) cloud-condensation nuclei derived by Aqua-MODIS during August 2007. The mean, standard deviation, maximum and minimum values correspond to the area 34.5°–38.5°N and 18°–22° E. The scatter plot (e) of AOD_{550} vs $\alpha_{550-865}$ corresponds to values obtained over the area 32.5°–40.5°N and 14.5°–24.5° ($N = 71$ pixels) on 25 August 2007.

biomass burning. Remer et al. (1998) found good correlation between biomass-burning AOD and columnar water vapor in the savanna regions of Brazil. In the present study the water-vapor content obtained from MODIS in NIR presented a low value on 25 August when the fire intensity was maximum (Fig. 4b). Therefore, the AOD vs water vapor plot presents a negative correlation during the fire season. This is probably attributed to the water evaporation caused by the elevated ambient temperature during the burning period. The aerosol-mass concentration (Fig. 4c) presents a similar day-to-day variability with that of AOD_{550} with larger values during the burning period. On 25 August, the maximum mass concentration over the affected pixels by the smoke plume reached 60 $\mu g\ cm^{-3}$. Badarinath et al. (2009b) found that the accumulation-mode particle loading was 14 times higher during a burning day (260 $\mu g\ m^{-3}$) compared to the background conditions (19 $\mu g\ m^{-3}$).

Aerosols emitted from biomass burning are a major source of CCN (e.g. Brioude et al., 2009); CCN, in turn, affects the microphysics of clouds and the radiation budget of the earth by increasing the cloud albedo (Penner and Novakov, 1996). To this respect, several studies have used MODIS CCN values (e.g. Gassó and Hegg, 2003; Andreae, 2008; Li et al., 2010) for investigating the aerosol–cloud interactions with satisfactory results and accuracy. In the burning period CCN increased dramatically; on 25 August (Fig. 4d) CCN got its maximum value and became ten times larger than that in the pre-burning period providing large amounts of nuclei. Fig. 4e shows the relationship between AOD_{550} and $\alpha_{550-865}$ on 25 August. There is a tendency of increasing $\alpha_{550-865}$ as AOD_{550} increases. Similar plots of AOD vs α were observed over locations affected by biomass burning (Radhi et al., 2009), indicating the strong influence of the fresh-smoke fine particles on increased AOD values. On the other hand, coagulation involves the collision of smaller particles to form a smaller number of larger particles, without any mass increase. This is also likely to lead to an increase in AOD as the larger particles reflect more radiation back to space.

4.2. Spatial distribution of biomass-burning aerosol properties

The investigation of the optical properties of the biomass-burning aerosols is important for the study of atmospheric radiative processes (Badarinath et al., 2009a,b). The spatial distribution of the biomass-burning aerosol characteristics derived from OMI is shown in Fig. 5. The extinction optical depth represents the aerosol load in the atmosphere, while the absorption optical depth and the SSA constitute a measure of the aerosol capability to absorb light. The extinction optical depth (OMAERUV algorithm) presents its largest values over the burning areas in western Peloponnese and over the adjoining seas along the smoke-plume pathway (Fig. 5a). Large values are also observed near the African coast (south edges of the figure). The absorption optical depth (OMAERUV algorithm) exhibits a similar spatial distribution, further indicating that the emitted aerosols are of absorbing nature (Fig. 5b). The main aerosol released from biomass burning that causes large variations in the atmospheric chemistry and radiation budget, is the Black Carbon (BC), the optically absorbing part of the carbonaceous aerosols (Saha and Despiau, 2009). Absorption by BC lowers the aerosol SSA increasing the amount of radiation absorbed in the atmosphere (Haywood and Shine, 1997), while due to its large absorption it can offset the White House aerosol effect (Schwartz, 1996).

The sign of the aerosol forcing at TOA can change depending on SSA (e.g. Takemura et al., 2003). During the period 24–27 August, the mean SSA (OMAERUV algorithm) was between ~0.8 and 1.0 with an average value of 0.91 ± 0.09 over the studied area (Fig. 5c). The wide range of SSA values highlights the presence of aerosols from different sources and optical characteristics over an area where the contribution of natural and anthropogenic aerosols can be significant. As the distance from the fire locations and the time of the flaming phase increase, the initial biomass-burning characteristics (e.g. low SSA values) are misquoted after being coated with aerosols from different sources. Lower SSA values (~0.8–0.85) were observed over parts of western Peloponnese and in distinct areas along the smoke plume. The spatial distribution of SSA in general agrees with that of the absorption coefficient due to larger presence of the absorbing BC. Badarinath et al. (2009b) found that the share of BC to total aerosol-mass concentration was ~5% during normal days and ~14% during biomass-burning days. This fact strongly influenced SSA by further reducing it. As expected, the NO_2 column concentration is larger over the burned areas (Fig. 5d), as well as over Athens due to the presence of biomass burning and anthropogenic aerosols. A large NO_2 concentration is also observed in northern Greece caused by industrial emissions.

The AI spatial distribution clearly indicates the maximum aerosol load as well as its absorbing nature over the burned areas and along the smoke plume (Fig. 5e). Thus, very large AI values (>4.0) are observed over western Peloponnese and southern Ionian Sea. Large AI values are also shown in the southwestern part of the map, near the African coast, and are associated with smoke and dust particles. On the other hand, AI is near to zero over the sea not affected by the dust plume and over northern Greece, indicating the presence of non UV-absorbing aerosols (sea salt and anthropogenic sulfate).

The spatial distribution of the aerosol properties obtained from Aqua-MODIS is shown in Fig. 6. Large AOD_{550} values (Fig. 6a) are observed in western Peloponnese and over Ionian Sea caused by the intense smoke plume. The largest AOD_{550} values in the southwestern part of the map are attributed to the combined effect of smoke and dust aerosols, as shown by OMI. The other regions are relatively free from aerosols. Effective radius (R_{eff}) is also evaluated for each size distribution by the MODIS algorithm over ocean (Ichoku et al., 2004). R_{eff} is defined by the ratio of the total volume of the particles to their total surface area. The aerosol-size distribution suggests dominance of accumulation-mode particles (R_{eff} in the range 0.1–0.3) along with smoke plume from western Peloponnese to north Africa (Fig. 6b); the northern Ionian Sea presents significantly higher values. Similar particle-mode radius has been found in the Australian fires (Radhi et al., 2009). Similar distribution to R_{eff} is exhibited by the Ångström exponent, as obtained from the MODIS algorithm over ocean (Fig. 6c). Larger values, reaching 1.7, are observed along the smoke plume with a continuous decrease with distance from the burned areas due to the mixing processes in the atmosphere or to growing in size of the initial biomass-burning aerosols. On the other hand, over the sea regions not affected by the smoke plume, the $\alpha_{550-865}$ values are below 0.8 indicative of marine aerosols. Similarly, the wavelength exponent suggested large loading of small-sized particles during the burning period compared to pre- and post-burning periods in northeastern India (Badarinath et al., 2004), in African savanna (Eck et al., 2001, 2003), and in Amazonia (Reid et al., 1999).

The spatial distribution of the aerosol-mass concentration (Fig. 6d) follows that of AOD_{550}, exhibiting larger values over Peloponnese (affected by soot particles), in the southwestern part of the map (affected by both smoke and dust) and over northwestern Ionian Sea close to Italy (affected by anthropogenic emissions). On the other hand, aerosols have an indirect effect on climate by increasing cloud albedo and cloud lifetime (Lohmann and Feichter, 2005). The intense smoke plume is responsible for the formation of additional CCN along its pathway as clearly shown from MODIS observations (Fig. 6e). Areas not affected by the smoke plume present background CCN values. The increase in CCN due to the release of biomass-burning aerosols might have significant impact on the regional climate at least in a limited time interval. In contrast, the absorbing aerosols warm the atmosphere, leading to

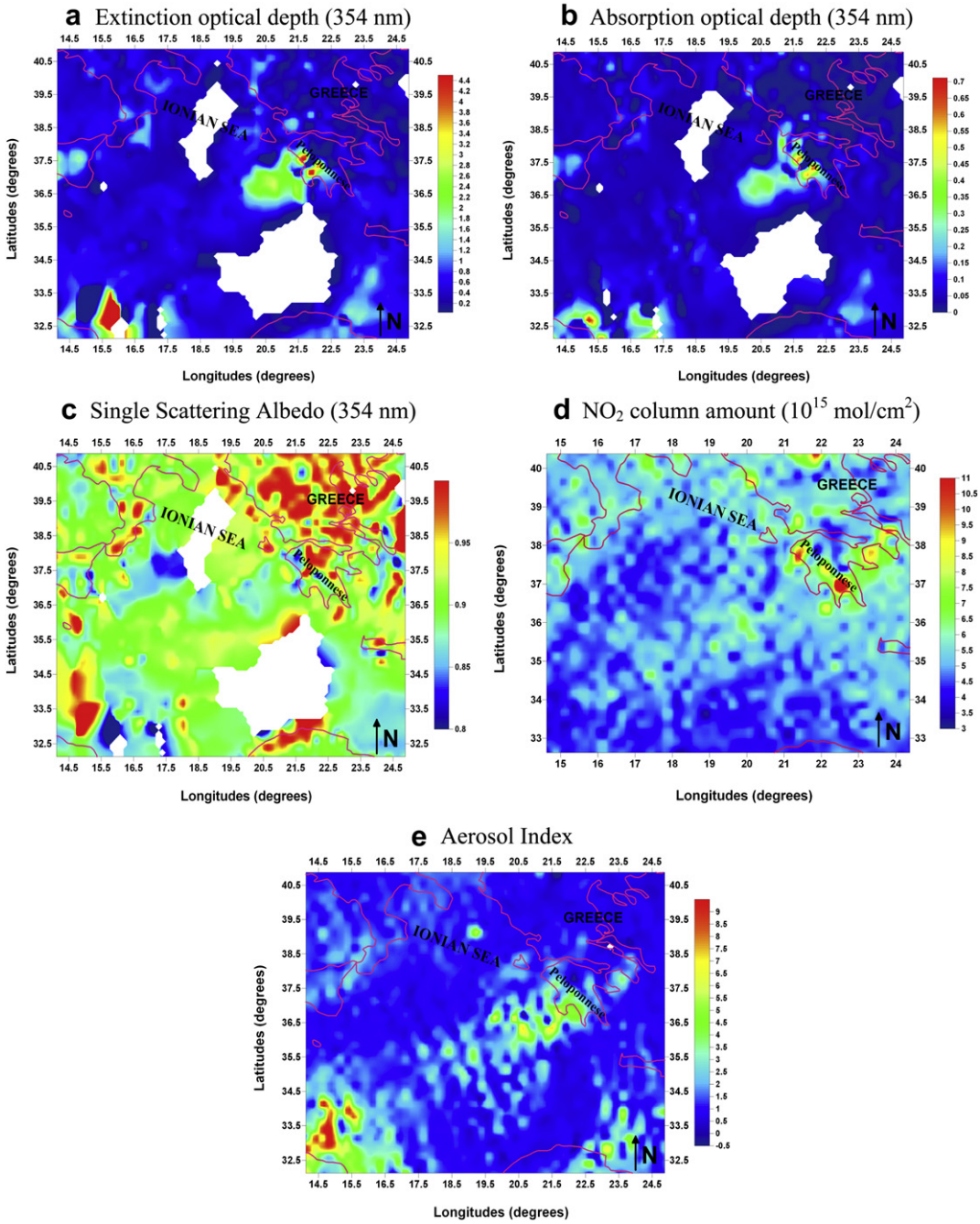

Fig. 5. Spatial distribution of (a) extinction optical depth, (b) absorption optical depth, (c) single scattering albedo, (d) NO_2 tropospheric column, and (e) AI derived by OMI. The mean values in the period 24–27 August 2007 were used. The white areas correspond to lack of data.

suppression of precipitation due to evaporation of clouds. However, during the burning period no cloud formation was detected in order to verify or not the above findings.

The Greek wildfires of August 2007 released large amounts of CO in the atmosphere, which strongly affected air pollution over southern Greece and Mediterranean. CO is a major trace gas with lifetime of several weeks. Fig. 7 shows the MOPITT CO distribution during the intense fire period (24–27 August 2007). Large CO amount ($\sim 2.4 \times 10^{18}$ Mol cm^{-2}) is observed over western Peloponnese, Athens and southern Ionian Sea following the transport of the smoke plume. Extremely large CO amounts ($>3.0 \times 10^{18}$ Mol cm^{-2}) were detected at the Libyan coast highlighting both the intensity of the fires and their impact over an extended area in Mediterranean. It was found that in the beginning of the fires (23–24 August) the large CO amount was detected above the fire locations; on the next days the CO plume was extended in a wide area covering the larger part of the central Mediterranean, also influencing strongly the north African coast. Using the Infrared Atmospheric Sounding Interferometer (IASI) retrievals Turquety et al. (2009) observed large CO plumes above Mediterranean and north Africa with total CO columns exceeding 24×10^{18} modecules cm^{-2} on 25 August 2007. They also found CO values up to 30×10^{18} modecules cm^{-2} close to the fire locations, but with larger uncertainty, corresponding to 0.321 Tg or ~40% of the total annual CO anthropogenic emissions in Greece; the present CO distribution agrees with that of IASI. The CO distribution is also in good agreement with the MODIS and OMI observations. The Cloud-

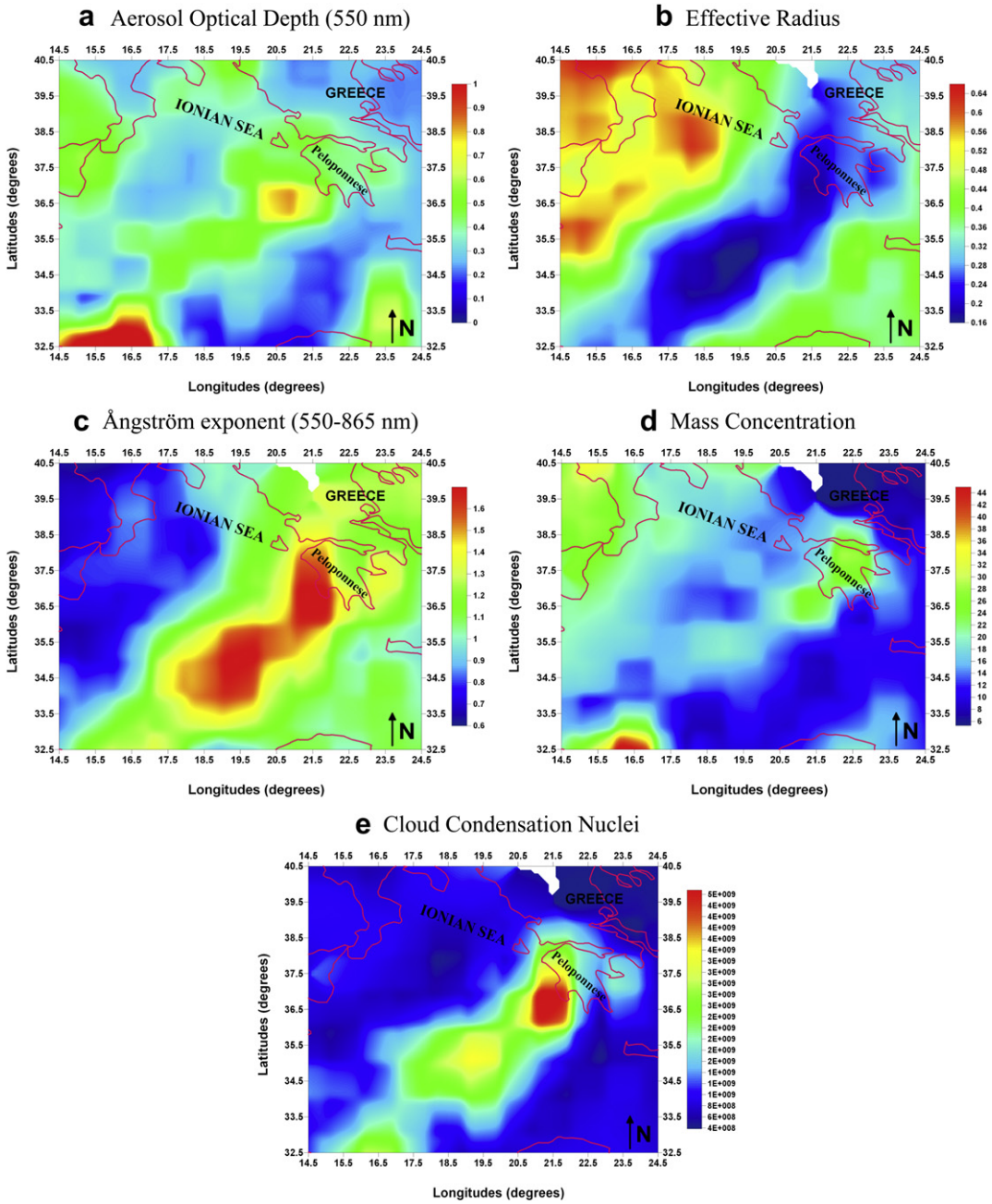

Fig. 6. Spatial distribution of (a) AOD_{550}, (b) effective radius, (c) $\alpha_{550-865}$, (d) aerosol-mass concentration, and (e) CCN derived by MODIS. The mean values in the period 24–27 August 2007 were used. The white areas correspond to lack of data.

Aerosol Lidar and Infrared Pathfinder Satellite Observation (CALIPSO) (Vaughan et al, 2004) detected an intense aerosol plume at 1–3 km on 25 August 2007, with backscatter coefficient of $\sim 4 \times 10^{-6}$ m^{-1} sr^{-1} (Turquety et al., 2009), which is similar in magnitude to that observed over Athens during intense biomass-burning episodes (Tsaknakis et al., 2010).

4.3. Radiative forcing of biomass-burning aerosols

The satellite-derived aerosol optical properties were inserted in a radiative transfer model to estimate the aerosol radiative forcing (ARF) at the surface, at TOA and within the atmosphere. MODIS-derived values of AOD, SSA and asymmetry factor (g) were used as inputs to the Santa Barbara Discrete-ordinate Atmospheric Radiative Transfer code (Ricchiazzi et al., 1998). ARF estimation depends on the surface reflectance, meteorological conditions, columnar water vapor and total ozone column (McComiskey et al., 2008). MODIS-derived precipitable water content and OMI-derived total ozone column were also used. Surface albedo contributes to ARF uncertainties (up to 10%) (Bellouin et al., 2004), while the ocean surface albedo taken from Tanré et al. (1990) was used. Though anisotropy of the ocean surface albedo is highly zenith-angle dependent, its effects are negligible for diurnally-averaged ARF estimations (Bellouin et al., 2004; Moorthy et al., 2009).

Fig. 8 shows the shortwave ARF at surface, TOA and within the atmosphere from SBDART model. The radiative transfer computations were performed for the wavelength range 0.25–4.0 μm as a function of solar zenith angle and the resulting fluxes were

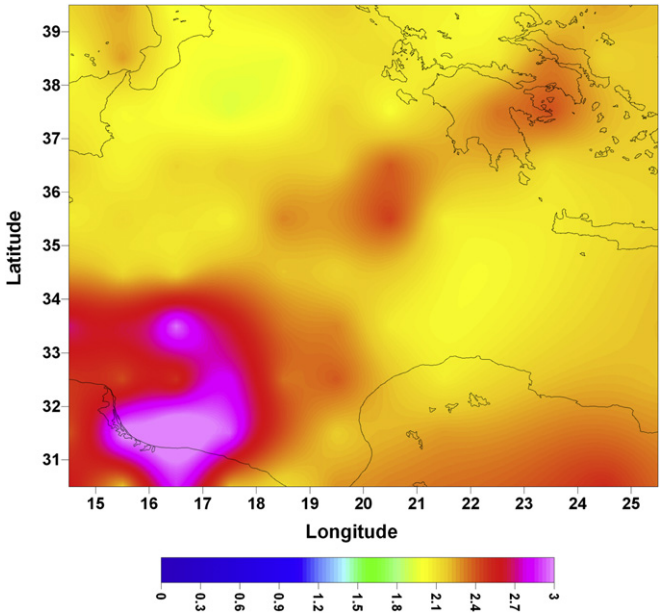

Fig. 7. Spatial distribution of total column CO (10^{18} Mol cm^{-2}) derived by MOPITT during the period 24–27 August 2007.

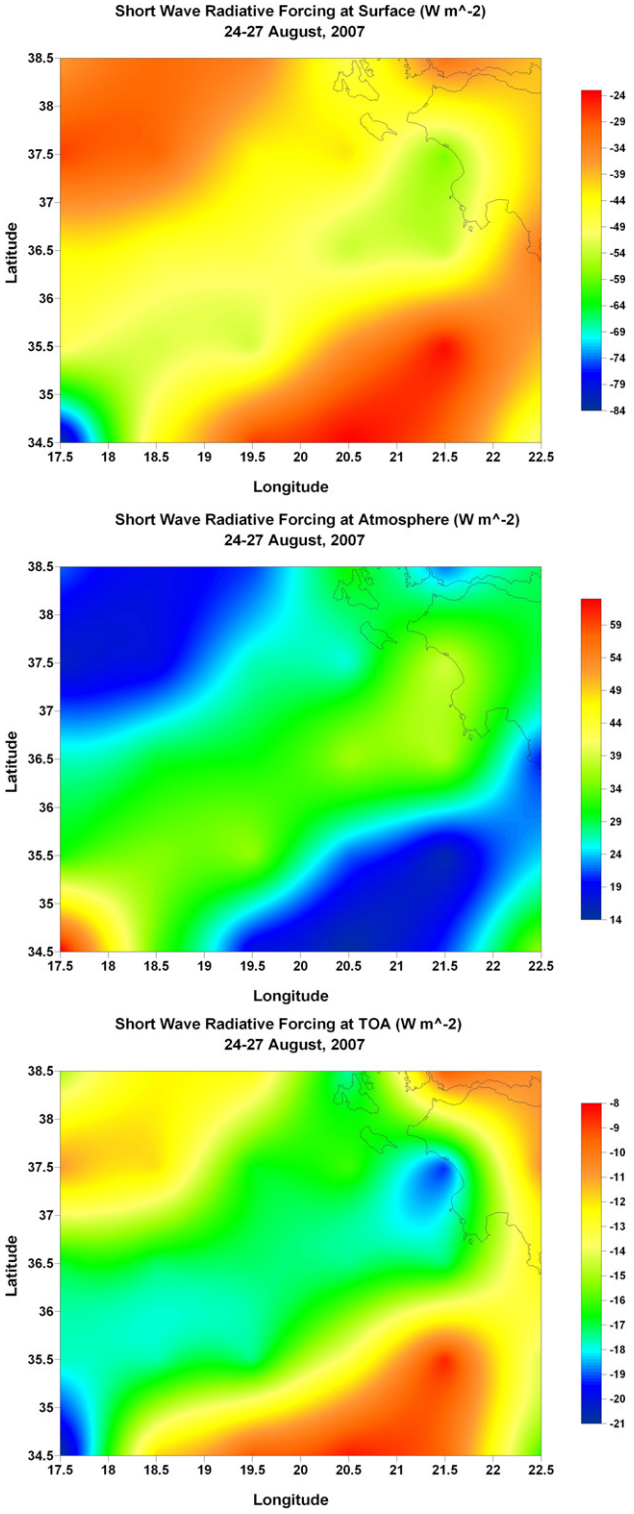

Fig. 8. Spatial distribution of the shortwave aerosol radiative forcing at surface, atmosphere and TOA as calculated by the SBDART model during the period 24–27 August 2007.

diurnally-averaged. The area covers western Peloponnese and southern Ionian Sea during the burning period (24–27 August 2007). A significant reduction in surface-reaching solar radiation occurs above the area covered by the smoke plume. This reduction ranges from −50 to −60 W m^{-2} and is comparable in magnitude with the radiative forcing caused by biomass-burning aerosols in Amazonia during SCAR-B campaign (Kaufman, 1998) and south Africa during SAFARI campaign (Eck et al., 2003). Such a strong attenuation of solar radiation by biomass-burning aerosols was also reported by Badarinath et al. (2009b) who found a reduction of 0.36 MEDh^{-1} in ground-reaching UV-erythemal radiation during burning days in northeastern India. More negative forcing values (~−80 W m^{-2}) are observed in the lower left part of the figure near the African coast; note also that above this area the AOD and the aerosol-mass concentration are very large (Fig. 6a and d). Diurnal average values of surface ARF caused by biomass-burning aerosols varied from −59 to −87 W m^{-2} on different days over India (Badarinath et al., 2009a) in close agreement with the present results. The biomass-burning aerosols also cause a significant heating in the lower atmosphere due to their ability to absorb solar light. Thus, the shortwave ARF is positive within the atmosphere causing atmospheric heating. The larger values of the heating are observed along the smoke plume and are more pronounced (50–60 W m^{-2}) near the African coast due to larger aerosol load and the absorbing nature of the aerosols. A large atmospheric heating (from ~35–40 W m^{-2}) is observed near the burning areas continuously decreasing in the far Ionian Sea. The values of atmospheric heating are in close agreement with those observed during the forest fires in Amazonia and south Africa. Compared to other natural aerosols, smoke and soot particles are generally smaller in size and more absorbing at visible and IR wavelengths (Dubovik et al., 2002). This results in increased atmospheric heating along with decreased incident solar radiation on the ground and some greenhouse trapping of the outgoing thermal radiation (Christopher et al., 2003). However, the aerosol impact on the radiation budget and climate is considered at TOA corresponding to the net ARF (surface and atmosphere). The sign of this forcing designates the cooling or heating effect of aerosols on regional or global scale. The TOA ARF during the burning period shows negative values (~−20 W m^{-2}) over the areas covered by the smoke plume and less negative values (−8 to −13 W m^{-2}) over areas free of biomass-burning aerosols. This is translated in an overall regional cooling since more solar radiation is scattered back to space. The results of numerous studies in the past (see the review by Satheesh and Krishnamoorthy, 2005) showed that the TOA

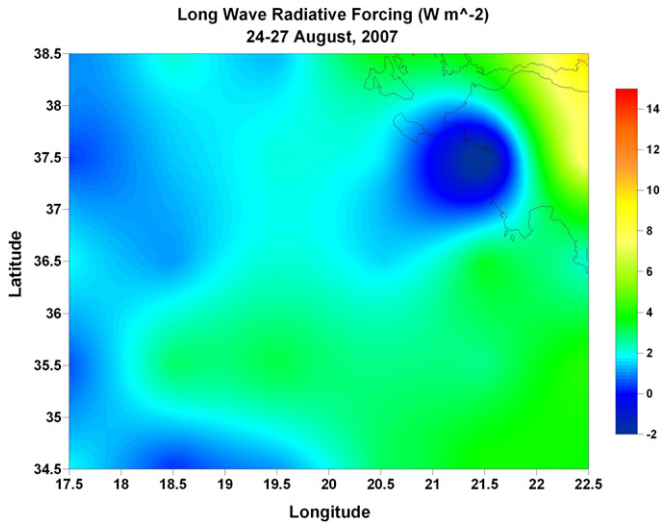

Fig. 9. Spatial distribution of the longwave aerosol radiative TOA forcing during 24–27 August 2007 as generated by the Atmospheric Infrared Sounder (AIRS) data.

forcing of biomass burning and soot aerosols is rather positive having a significant uncertainty (0.3 ± 0.8); this is interpreted as an overall heating above the areas affected by biomass burning. In the present study the results of the SBDART model showed a cooling effect of the biomass-burning aerosols possibly caused by sulfate particles and the very thick smoke plumes, which strongly scatter solar radiation back to space. On the other hand, negative TOA ARF values were observed in Amazonian fires during SCAR-B (Kaufman, 1998), which agree with the present results. However, the estimated values of ARF strongly depend on the values of SSA and surface albedo, which could cause errors in the calculations (Kim and Ramanathan, 2008).

The spatial distribution of the TOA longwave ARF during 24–27 August 2007 is shown in Fig. 9. The image was generated using the Atmospheric Infrared Sounder (AIRS) data (McMillan et al., 2008). The longwave ARF from AIRS was calculated via the difference of AIRS longwave radiations pre (20–23 August) and during (24–27 August) forest fires. During the fire period, the reduction in longwave radiation over western Peloponnese is very clear, indicating negative forcing, and thus, cooling due to enhanced AOD values from the forest fires. However, the longwave ARF is about ten times lower than the shortwave one, and, therefore, it does not play such an important role in the regional radiation balance.

5. Conclusions

Devastating fires affected Greece in the summer of 2007, with the loss of more than 60 human lives, the destruction of more than 100 villages and hundreds of square kilometers of burned forested areas. The present study captured the burned areas over Peloponnese using remote-sensing observations of high spatial resolution (FORMOSAT-2). The aerosol properties derived from MODIS and OMI suggested large amounts of biomass-burning aerosols over the burned areas, which were transported thousands of kilometers downwind. The forest fires caused large effects both on the aerosol amount (AOD, mass concentration, AI) and the aerosol properties and size (Ångström exponent, effective radius, absorption optical depth, CCN); they also affected strongly the regional climate and alterered provisionally the radiation balance. The biomass-burning aerosols are smaller in size and more absorbing at solar and IR wavelengths compared to the anthropogenic and natural aerosols. This resulted in increased atmospheric heating and decreased incident solar radiation on the ground. The SBDART calculations on ARF at the surface were found to range from ~ -50 to -60 W m^{-2} in western Peloponnese during the forest-fire period resulting in significant cooling at the surface. The atmospheric heating was also large, ranging from $\sim$35 to 40 W m^{-2} over and close to the forest-fires locations. The combination of both resulted in an overall net regional cooling at the TOA with negative forcing values from -17 to -20 W m^{-2}. The intense smoke plumes and their long-range transport strongly affected the radiation budget not only over the fire locations, but also over an extended area in the central Mediterranean during August 2007. Monitoring of the forest fires and the associated emissions of aerosols over the Greek region needs more attention to understand the cause-effect scenarios. Conventional methods in quantification of aerosols involving ground inventory aided with information given by remotely-sensed data from space-borne sensors are capable of addressing the problem with good scientific and technical strength.

Acknowledgments

The authors would like to thank MODIS and OMI scientific teams (past and present) for processing data via Giovanni website (http://giovanni.gsfc.nasa.gov/). Furthermore, the NCEP/NCAR re-analysis is also gratefully acknowledged.

References

Atbd-OMI, August 2002. OMI algorithm theoretical basis document. In: Stammes, P., Noordhoek, R. (Eds.), Clouds, Aerosols, and Surface UV Irradiance, vol. III ATBD-OMI-03, Version 2.0.

Amiridis, V., Balis, D.S., Giannakaki, E., Stohl, A., Kazadzis, S., Koukouli, M.E., Zanis, P., 2009. Optical characteristics of biomass-burning aerosols over Southeastern Europe determined from UV-Raman lidar measurements. Atmospheric Chemistry and Physics 9, 2431–2440.

Andreae, M.O., Merlet, P., 2001. Emission of trace gases and aerosols from biomass burning. Global Biogeochemical Cycles 15, 955–966.

Andreae, M.O., 2008. Correlation between cloud condensation nuclei concentration and aerosol optical thickness in remote and polluted regions. Atmospheric Chemistry and Physics Discussions 8, 11293–11320.

Arola, A., Kazadzis, S., Lindfors, A., Krotkov, N., Kujanpää, J., Tamminen, J., Bais, A., Di Sarra, A., Villaplana, J.M., Brogniez, C., Siani, A.M., Janouch, M., Weihs, P., Webb, A., Koskela, T., Kouremeti, N., Meloni, D., Buchard, V., Auriol, F., Ialongo, I., Staneck, M., Simic, S., Smedley, A., Kinne, S., 2009. A new approach to correct for absorbing aerosols in OMI UV. Geophysical Research Letters 36, L22805. doi:10.1029/2009GL041137.

Badarinath, K.V.S., Madhavi Latha, K., Kiran Chand, T.R., Gupta, P.K., Ghosh, A.B., Jain, S.L., Gera, B.S., Singh, R., Sarkar, A.K., Singh, N., Parmar, R.S., Koul, S., Kohli, R., Nath, S., Ojha, V.K., Singh, G., 2004. Characterization of aerosols from biomass burning – a case study from Mizoram (Northeast), India. Chemosphere 54, 167–175.

Badarinath, K.V.S., Kharol, S.K., Sharma, A.R., 2009a. Long-range transport of aerosols from agriculture crop residue burning in Indo-Gangetic Plains – a study using LIDAR, ground measurements and satellite data. Journal of Atmospheric and Solar Terrestrial Physics 71, 112–120.

Badarinath, K.V.S., Madhavi Latha, K., Kiran Chand, T.R., Gupta, P.K., 2009b. Impact of biomass burning on aerosol properties over tropical wet evergreen forests of Arunachal Pradesh, India. Atmospheric Research 91, 87–93.

Balis, D.S., Amiridis, V., Zerefos, C.S., Gerasopoulos, E., Andrae, M., Zanis, P., Kazantzidis, A., Kazadzis, S., Papayannis, A., 2003. Raman lidar and sunphotometric measurements of aerosol optical properties over Thessaloniki, Greece during a biomass-burning episode. Atmospheric Environment 37, 4529–4538.

Bellouin, N., Boucher, O., Vesperini, M., Tanré, D., 2004. Estimating the direct aerosol radiative perturbation: impact of ocean surface representation and aerosol nonsphericity. Quarterly Journal of Royal Meteorological Society 130, 2217–2232.

Boschetti, L., Roy, D., Barbosa, P., Boca, R., Justice, C., 2008. A MODIS assessment of the summer 2007 extent burned in Greece. International Journal of Remote Sensing 29 (8), 2433–2436.

Brioude, J., Cooper, O.R., Feingold, G., Trainer, M., Freitas, S.R., Kowal, D., Ayers, J.K., Prins, E., Minnis, P., McKeen, S.A., Frost, G.J., Hsieet, E.-Y., 2009. Effect of biomass burning on marine stratocumulus clouds off the California coast. Atmospheric Chemistry and Physics 9, 8841–8856.

Christopher, S.A., Wang, J., Ji, Q., Tsay, S.i.C.h.e.e., 2003. Estimation of diurnal shortwave dust aerosol radiative forcing during PRIDE. Journal of Geophysical Research 108 (D19), 8596.

Curier, R.L., Veefkind, J.P., Braak, R., Veihelmann, B., Torres, O., de Leeuw, G., 2008. Retrieval of aerosol optical properties from OMI radiances using

a multiwavelength algorithm: application to western Europe. Journal of Geophysical Research 113, D17S90. doi:10.1029/2007JD008738.
Dubovik, O., Holben, B.N., Eck, T.F., Smirnov, A., Kaufman, Y.J., King, M.D., Tanrè, D., Slutsker, I., 2002. Variability of absorption and optical properties of key aerosol types observed in worldwide locations. Journal of Atmospheric Science 59, 590–608.
Eck, T.F., Holben, B.N., Ward, D.E., Dubovic, O., Reid, J.S., Smirnov, A., Mukelabai, M.M., Hsu, N.C., O' Neil, N.T., Slutsker, I., 2001. Characterization of the optical properties of biomass-burning aerosols in Zambia during the 1997 ZIBBEE field campaign. Journal of Geophysical Research 106 (D4), 3425–3448.
Eck, T.F., Holben, B.N., Ward, D.E., Mukelabai, M.M., Dubovik, O., Smirnov, A., Schafer, J.S., Hsu, N.C., Piketh, S.J., Queface, A., Le Roux, J., Swap, R.J., Slutsker, I., 2003. Variability of biomass-burning aerosol optical characteristics in southern Africa during SAFARI 2000 dry season campaign and a comparison of single scattering albedo estimates from radiometric measurements. Journal of Geophysical Research 108 (D13), 8477.
Emmons, L.K., Pfister, G.G., Edwards, D.P., Gille, J.C., Sachse, G.W., Blake, D.R., Wofsy, S., Gerbig, C., Matross, D., Nédélec, P., 2007. Measurements of pollution in the troposphere (MOPITT) validation exercises during summer 2004 field campaigns over North America. Journal of Geophysical Research 112 (12), D12S02. doi:10.1029/2006JD007833.
Founda, D., Giannakopoulos, C., 2009. The exceptionally hot summer of 2007 in Athens, Greece – a typical summer in the future climate? Global Planetary Change 67, 227–236.
Gassó, S., Hegg, D.A., 2003. On the retrieval of columnar aerosol mass and CCN concentration by MODIS. Journal of Geophysical Research 108, D14010. doi:10.1029/2002JD002382.
Giglio, L., Descloitres, J., Justice, C.O., Kaufman, Y., 2003. An enhanced contextual fire detection algorithm for MODIS. Remote Sensing of Environment 87, 273–282.
Haywood, J.M., Shine, K.P., 1997. Multi-spectral calculations of the radiative forcing of tropospheric sulphate and soot aerosols using a column model. Quarterly Journal of Royal Meteorological Society 123, 1907–1930.
Hellas, W.W.F., 2008. Ecological report of the Peloponnesian wildfires in August 2007 (http://www.env-edu.gr/Documents/FIRE_report_Peloponnisos.pdf) in Greek.
Ichoku, C., Kaufman, Y.J., Remer, L.A., Levy, R., 2004. Global aerosol remote sensing from MODIS. Advances in Space Research 34, 820–827.
Kambezidis, H.D., Kaskaoutis, D.G., Kassomenos, P., Melas, D., Papadopoulos, A., Yeniguin, O., Im, U., Onay, T., Topcu, S., Incecik, S., 2006. An investigation on forest-fire risk assessment in selected areas in Greece and Turkey. Forest Ecology and Management 234 (Suppl. 1), S.46.
Kasischke, E.S., Hyer, E.J., Novelli, P.C., Bruhwiler, L.P., French, N.H.F., Sukhinin, A.I., Hewson, J.H., Stocks, B.J., 2005. Influences of boreal fire emissions on Northern Hemisphere atmospheric carbon and carbon monoxide. Global Biogeochemical Cycles 19, GB1012. doi:10.1029/2004GB002300.
Kaskaoutis, D.G., Kambezidis, H.D., Hatzianastassiou, N., Kosmopoulos, P.G., Badarinath, K.V.S., 2007. Aerosol climatology: dependence of the Ångström exponent on wavelength over four AERONET sites. Atmospheric Chemistry and Physics Discussions 7, 7347–7397.
Kaufman, Y.J., 1998. Smoke, clouds and radiation-Brazil (SCAR-B) experiment. Journal of Geophysical Research 31, 103–108.
Kim, D., Ramanathan, V., 2008. Solar radiation budget and radiative forcing due to aerosols and clouds. Journal of Geophysical Research 113 (2), D02203.
Kontoes, H., Sifakis, N., Keramitsoglou, I., Pafili, M., Palas, T.h., Balatsos, P. (Eds.), 2008. Geoinformation Services for Natural Disasters: Assessment of 2007 Burnt Areas in Greece Using Satellite Data A publication of the Hellenic Ministry of Rural Development and Food reporting on the methods and results of the ESA RISK EOS/GMES-Service Element (Extension to Greece), Athens.
Kontoes, H., Sifakis, N., Keramitsoglou, I., 2009. GMES burn scar mapping kicks into full gear after 2007 wildfires in Greece. Window on GMES: discover how GMES is turning into reality – success stories, BOSS4GMES (pub.). (issue 3), pp. 64–69 (ISSN 2030-5419).
Levy, R.C., Remer, L.A., Mattoo, S., Vermote, E., Kaufman, Y.J., 2007. Second-generation operational algorithm: retrieval of aerosol properties over land from inversion of moderate resolution imaging spectroradiometer spectral reflectance. Journal Geophysical Research 112, D13211. doi:10.1029/2006JD007811.
Levelt, P.F., Hilsenrath, E., Leppelmeier, G.W., van den Oord, G.H.J., Bhartia, P.K., Tamminen, J., de Haan, J.F., Veefkind, J.P., 2006. Science objectives of the ozone monitoring instrument. IEEE Transactions of Geosciences and Remote Sensing 44, 1199–1208. doi:10.1109/TGRS.2006.872336.
Li, R., Min, Q.-L., Harrison, L.C., 2010. A case study: the indirect aerosol effects of mineral dust on warm clouds. Journal of Atmospheric Science 67, 805–816.
Liu, Y., Kahn, R.A., Chaloulakou, A., Koutrakis, P., 2009. Analysis of the impact of the forest fires in august 2007 on air quality of Athens using multi-sensor aerosol remote sensing data, meteorology and surface observations. Atmospheric Environment 43, 3310–3318.
Lohmann, U., Feichter, J., 2005. Global indirect aerosol effects: a review. Atmospheric Chemistry and Physics 5, 715–737.
McMillan, W.W., Warner, J.X., McCourt Comer, M., Maddy, E., Chu, A., Sparling, L., Eloranta, E., Hoff, R., Sachse, G., Barnet, C., Razenkov, I., Wolf, W., 2008. AIRS views transport from 12 to 22 July 2004 Alaskan/Canadian fires: correlation of AIRS CO and MODIS AOD with forward trajectories and comparison of AIRS CO retrievals with DC-8 in situ measurements during INTEX-A/ICARTT. Journal of Geophysical Research 113 (20), D20301. doi:10.1029/2007JD009711.
Minchella, A., Del Frate, F., Capogna, F., Anselmi, S., Manes, F., 2009. Use of multitemporal SAR data for monitoring vegetation recovery of Mediterranean burned areas. Remote Sensing of Environment 113, 588–597.
Moorthy, K.K., Nair, V.S., Babu, S.S., Satheesh, S.K., 2009. Spatial and vertical heterogeneities in aerosol properties over oceanic regions around India: implications for radiative forcing. Quarterly Journal of Royal Meteorological Society 135, 2131–2145.
McComiskey, A., Schwartz, S.E., Schmid, B., Guan, H., Lewis, E.R., Richiazzi, P., Ogren, J.A., 2008. Direct aerosol forcing: calculation from observables and sensitivities to inputs. Journal of Geophysical Research 113, D09202. doi:10.1029/2007JD009170.
Nastos, P.T., Philandras, C.M., Repapis, C.C., 2002. Application of canonical analysis to air temperature and precipitation regimes over Greece. Fresenius Environmental Bulletin 11, 488–493.
Penner, J.E., Novakov, T., 1996. Carbonaceous particles in the atmosphere: a historical perspective to the fifth international conference on carbonaceous particles in the atmosphere. Samples by thermal evolution. Analytical Chemistry 54, 1627–1630.
Radhi, M., Box, M.A., Box, G.P., Gupta, P., Christopher, S.A., 2009. Evolution of the optical properties of biomass-burning aerosol during the 2003 southeast Australian bushfires. Applied Optics 48, 1764–1773.
Reid, J.S., Eck, T.F., Christopher, S.A., Hobbs, P.V., Holben, B.N., 1999. Use of the Ångström exponent to estimate the variability of optical and physical properties of aging smoke particles in Brazil. Journal of Geophysical Research 104 (D22), 27473–27489.
Remer, L.A., Kaufman, Y., Holben, B.N., Thompson, A.M., McNamara, D.P., 1998. Biomass-burning aerosol size distribution and modeled optical properties. Journal of Geophysical Research 103, 31879–31891.
Remer, L.A., Kaufman, Y.J., Tanre, D., Mattoo, S., Chu, D.A., Martins, J.V., Li, R.-R., Ichoku, C., Levy, R.C., Kleidman, R.G., Eck, T.F., Vermote, E., Holben, B.N., 2005. The MODIS aerosol algorithm, products, and validation. Journal of Atmospheric Science 62, 947–973.
Ricchiazzi, P., Yang, S., Gautier, C., Sowle, D., 1998. SBDART: a research and teaching software tool for plane-parallel radiative transfer in the earth's atmosphere. Bulletin of American Meteorological Society 79 (10), 2101–2114.
Roy, D.P., Jin, Y., Lewis, P.E., Justice, C.O., 2005. Prototyping a global algorithm for systematic fire affected area mapping using MODIS time series data. Remote Sensing of Environment 97, 137–162.
Saha, A., Despiau, S., 2009. Seasonal and diurnal variations of black carbon aerosols over a Mediterranean coastal zone. Atmospheric Research 92, 27–41.
Satheesh, S.K., Krishnamoorthy, K., 2005. Radiative effects of natural aerosols: a review. Atmospheric Environment 35, 2089–2110.
Schwartz, S.E., 1996. The white house effect-short wave radiative forcing of climate by anthropogenic aerosols – an overview. Journal of Aerosol Science 27, 359–382.
Takemura, T., Nakajima, T., Higurashi, A., Ohta, S., Sugimoto, N., 2003. Aerosol distributions and radiative forcing over the Asian Pacific region simulated by spectral radiation-transport model for aerosol species (SPRINTARS). Journal of Geophysical Research 108 (D23), 8659. doi:10.1029/2002JD003210.
Tanré, D., Deroo, C., Duhaut, P., Herman, M., Morcrette, J.J., Perbos, J., Deschamps, P.Y., 1990. Description of a computer code to simulate the satellite signal in the solar spectrum: the 5S code. International Journal of Remote Sensing 11, 659–668.
Tanré, D., Kaufman, Y.J., Herman, M., Mattoo, S., 1997. Remote sensing of aerosol properties over oceans using the MODIS/EOS spectral radiances. Journal of Geophysical Research 102, 16,971–16,988.
Torres, O., Bhartia, P.K., Herman, J.R., Ahmad, Z., Gleason, J., 1998. Derivation of aerosol properties from satellite measurements of backscattered ultraviolet radiation: theoretical basis. Journal of Geophysical Research 103, 17099–17110.
Tsaknakis, G., Mamouri, R.E., Papayannis, A., Amiridis, V., Kokkalis, P., 2010. Optical properties of biomass-burning aerosols in respect to their source distance over Athens, Greece using a 6-wavelength raman lidar system. In: Proceedings of the 25th International Laser Remote Sensing Conference, St. Petersburg, Russia, July 5–9, 2010.
Turquety, S., Clerbaux, C., Law, K., Coheur, P.-F., Cozic, A., Szopa, S., Hauglustaine, D.A., Hadji-Lazaro, J., Gloudemans, A.M.S., Schrijver, H., Boone, C.D., Bernath, P.F., Edwards, D.P., 2008. CO emission and export from Asia: an analysis combining complementary satellite measurements (MOPITT, SCIAMACHY and ACE-FTS) with global modeling. Atmospheric Chemistry and Physics 8, 5187–5204.
Turquety, S., Hurtmans, D., Hadji-Lazaro, J., Coheur, P.-F., Clerbaux, C., Josset, D., Tsamalis, C., 2009. Tracking the emission and transport of pollution from wildfires using the IASI CO retrievals: analysis of the summer 2007 Greek fires. Atmospheric Chemistry and Physics 9, 4897–4913.
Veraverbeke, S., Lhermitte, S., Verstraeten, W.W., Goossens, R., 2010a. The temporal dimension of differenced Normalized Burn Ratio (dNBR) fire/burn severity studies: the case of the large 2007 Peloponnese wildfires in Greece. Remote Sensing of Environment 114, 2548–2563.
Veraverbeke, S., Verstraeten, W.W., Lhermitte, S., Goossens, R., 2010b. Evaluation Landsat Thematic Mapper spectral indices for estimating burn severity of the 2007 Peloponnese wildfires in Greece. International Journal Wildland Fire 19, 558–569.
Vaughan, M.A., Young, S.A., Winker, D.M., Powell, K.A., Omar, A.H., Liu, Z., Hu, Y., Hostetler, C.A., 2004. Fully automated analysis of space-based lidar data: an overview of the CALIPSO retrieval algorithms and data products. Proceedings of SPIE 5575, 16–30.
Wang, L., Qu, J.J., Hao, X., 2008. Forest fire detection using the normalized multiband drought index (NMDI) with satellite measurements. Agricultural and Forest Meteorology 148, 1767–1776.
Westerling, A.L., Gershunov, A., Brown, T., Cayan, D., Dettinger, M., 2003. Climate and wildfire in the western United States. Bulletin of the American Meteorological Society 84, 595–604.